HHS Public Access

Author manuscript

Circ Res. Author manuscript; available in PMC 2017 January 22.

Published in final edited form as:

Circ Res. 2016 January 22; 118(2): e19–e28. doi:10.1161/CIRCRESAHA.115.307919.

Multimodal SHG-2PF Imaging of Microdomain Ca^{2+}-Contraction Coupling in Live cardiac myocytes

Samir Awasthi[1,3], **Leighton T. Izu**[2], **Ziliang Mao**[1], **Zhong Jian**[2], **Trevor Landas**[2], **Aaron Lerner**[1], **Rafael Shimkunas**[3], **Rahwa Woldeyesus**[3], **Julie Bossuyt**[2], **Brittani Wood**[2], **Yi-Je Chen**[2,5], **Dennis L. Matthews**[1], **Deborah K. Lieu**[6], **Nipavan Chiamvimonvat**[6], **Kit S. Lam**[4,7], **Ye Chen-Izu**[2,3,6], and **James W. Chan**[1,8]

[1]Center for Biophotonics, UC Davis School of Medicine, University of California, Davis, 2700 Stockton Blvd., Sacramento, CA, 95817, USA

[2]Pharmacology, University of California, Davis, One Shields Ave., Davis, CA, 95616, USA

[3]Biomedical Engineering, University of California, Davis, One Shields Ave., Davis, CA, 95616, USA

[4]Biochemistry and Molecular Medicine, University of California, Davis, One Shields Ave., Davis, CA, 95616, USA

[5]Microsurgery Core, University of California, Davis, One Shields Ave., Davis, CA, 95616, USA

[6]Division of Cardiology, Department of Internal Medicine, UC Davis School of Medicine, 4150 V St., Sacramento, CA, 95817, USA

[7]Division of Hematology/Oncology, Department of Internal Medicine, UC Davis School of Medicine, 4150 V St., Sacramento, CA, 95817, USA

[8]Department of Pathology and Laboratory Medicine, UC Davis School of Medicine, 4400 V St., Sacramento, CA, 95817, USA

Abstract

Rationale—cardiac myocyte contraction is caused by Ca^{2+} binding to troponin C, which triggers the cross-bridge power stroke and myofilament sliding in sarcomeres. Synchronized Ca^{2+} release causes whole cell contraction and is readily observable with current microscopy techniques. However, it is unknown whether localized Ca^{2+} release, such as Ca^{2+} sparks and waves, can cause local sarcomere contraction. Contemporary imaging methods fall short of measuring microdomain Ca^{2+}-contraction coupling in live cardiac myocytes.

Objective—To develop a method for imaging sarcomere-level Ca^{2+}-contraction coupling in healthy and disease-model cardiac myocytes.

Address correspondence to: Dr. James W. Chan Associate Professor, Department of Pathology and Laboratory Medicine, University of California, Davis, 2700 Stockton Blvd., Suite 1400, Sacramento, CA 95817, Tel: (916) 734-0774, jwjchan@ucdavis.edu. Dr. Ye Chen-Izu, Associate Professor, Departments of Pharmacology, Bioengineering, Internal Medicine/Cardiology, University of California, Davis, 451 Health Science Dr., Tupper Hall 2221, Davis, CA 95616, USA, Tel: (530) 752-3232, ychenizu@ucdavis.edu. Y.C-I. and J.W.C. contributed equally to this study.

DISCLOSURES

None.

Methods and Results—Freshly isolated cardiac myocytes were loaded with the Ca^{2+}-indicator Fluo-4. A confocal microscope equipped with a femtosecond-pulsed near-infrared laser was used to simultaneously excite second harmonic generation (SHG) from A-bands of myofibrils and two-photon fluorescence (2PF) from Fluo-4. Ca^{2+} signals and sarcomere strain correlated in space and time with short delays. Furthermore, Ca^{2+} sparks and waves caused contractions in subcellular microdomains, revealing a previously underappreciated role for these events in generating subcellular strain during diastole. Ca^{2+} activity and sarcomere strain were also imaged in paced cardiac myocytes under mechanical load, revealing spontaneous Ca^{2+} waves and correlated local contraction in pressure overload-induced cardiomyopathy.

Conclusions—Multi-modal SHG-2PF microscopy enables the simultaneous observation of Ca^{2+} release and mechanical strain at the sub-sarcomere level in living cardiac myocytes. The method benefits from the label-free nature of SHG, which allows A-bands to be imaged independently of T-tubule morphology and simultaneously with Ca^{2+} indicators. SHG-2PF imaging is widely applicable to the study of Ca^{2+}-contraction coupling and mechano-chemo-transduction in both health and disease.

Keywords

Multimodality imaging; calcium sparks; calcium transients; contraction; coupling; second harmonic generation; two-photon fluorescence

INTRODUCTION

Excitation-contraction coupling in cardiac myocytes is mediated by Ca^{2+}. During systole, an action potential opens voltage-gated Ca^{2+} channels in the sarcolemma to allow Ca^{2+} entry into the cell, which triggers a much larger release of Ca^{2+} from the sarcoplasmic reticulum (SR) through the ryanodine receptor (RyR); this process is termed Ca^{2+}-induced Ca^{2+} release (CICR). Synchronous CICR throughout the cell increases the cytosolic Ca^{2+} concentration, and subsequent Ca^{2+} binding to troponin C causes conformational changes in contractile machinery that results in the cross-bridge power stroke and sarcomere contraction. During diastole, cytosolic Ca^{2+} is lowered to basal level by sequestration into the SR Ca^{2+} store and extrusion from the cell, resulting in sarcomere relaxation.[1]

The RyR cluster is the basic Ca^{2+} release unit (CRU) in cardiac myocytes. RyR responds to local rises in Ca^{2+} and opens in a stochastic manner. It opens and closes in an all-or-none fashion to release a quantum amount of Ca^{2+}, giving rise to a Ca^{2+} spark. The distribution of CRUs in cardiac myocytes shows a lattice-like registered pattern in alignment with sarcomere structure.[2,3] Synchronous opening of CRUs throughout the cell causes a uniform Ca^{2+} transient and coordinated whole-cell contraction. Asynchronous opening of RyRs, however, causes non-uniform rises of Ca^{2+} in local microdomains, manifesting as Ca^{2+} sparks and waves.[4–6] While healthy cardiac myocytes are largely quiescent and relaxed at rest, studies have shown that various pathological conditions can increase the occurrence of Ca^{2+} sparks and waves during diastole in cardiac myocytes.[7–11]

It is plausible that Ca^{2+} sparks and waves cause Ca^{2+} binding to troponin C and myofilament contraction in local sarcomeres, potentially increasing mechanical strain and

stress within the cardiac myocyte. Mechanical stress is linked to cardiac dysfunction and arrhythmias in conditions such as hypertension, myocardial infarction, atrial fibrillation (AF) and ventricular tachycardia/fibrillation (VT/VF).[12] Such links are well established at the whole heart level in clinical medicine, but the underlying cellular and molecular mechanisms remain unclear. We speculate that local non-uniform contraction may contribute to disease development via mechano-chemo-transduction pathways and by affecting cardiac myocyte contractility. It is therefore important to investigate local Ca^{2+} release and the mechanical response at the sarcomere level, constituting the basic unit of contraction.

Previously, several techniques have been used to measure sarcomere shortening during cardiac myocyte contraction, including cell-edge detection, sarcomere pattern analysis (using Fourier Transform/FFT or autocorrelation-based algorithms), T-tubule labeling with ANEP dyes[13] and quantum dots[14], and sarcomere structure labeling using genetic expression of fluorescent proteins[15]. However, each of those methods falls short of providing a practical and reliable method for measuring sarcomere contraction in sub-cellular microdomains. The video-based edge detection method measures cell contraction as the sum of all sarcomere contractions; local contraction cannot be isolated. Sarcomere pattern analysis measures an averaged sarcomere length from the FFT of many sarcomeres. T-tubule labeling methods cannot be applied to disease models in which the T-tubule distribution is irregular or detubulated, such as in heart failure.[16,17] Genetic labeling of the sarcomere with fluorescent proteins is labor-intensive, and some studies suggest that GFP directly affects cardiac myocyte contractility.[18–20] Moreover, genetic labeling needs to be executed and validated in each new disease model, which is non-trivial. The GFP spectrum also overlaps with the emission spectrum of commonly used Ca^{2+} indicators such as Fluo-3 and Fluo-4, and therefore interferes with high resolution Ca^{2+}-contraction imaging. Despite these drawbacks, these studies and others in skeletal muscle[21] have been able to show non-uniform sarcomere length changes in spatially uniform Ca^{2+} concentrations.

In this project, we develop an easy-to-use and widely applicable multimodal imaging technique to simultaneously image Ca^{2+} levels and sarcomere contraction at high spatial and temporal resolutions. We image sarcomere contraction in a *label-free* manner by using second harmonic generation (SHG) to track A-bands in sub-sarcomere structure in live cardiac myocytes. We further integrate SHG with two-photon fluorescence (2PF) microscopy to measure Ca^{2+} release. Importantly, the multimodal technique is superbly suited for imaging live cells in real time because SHG microscopy does not require the use of an exogenous label or genetic modification. Furthermore, a single laser can be used to excite SHG and 2PF, providing inherent spatial and temporal colocalization of the signals.

In what follows, we demonstrate how to use the technique to simultaneously image local Ca^{2+} signals and sarcomere contraction, and we also present the computational methods for data analysis. These provide a complete toolbox for using SHG-2PF microscopy to investigate various cell models. We then use the multimodal technique to reveal that localized Ca^{2+} release events can cause local sarcomere contractions in sub-cellular microdomains in both healthy and diseased cells. Specifically, a Ca^{2+} spark can cause sarcomere contraction (termed *myo-pinch*) and a Ca^{2+} wave can cause sequential contraction

of adjacent sarcomeres. We also apply the SHG-2PF method to image aberrant Ca^{2+} and contractions in paced cardiac myocytes under mechanical load. The data reveal a phenomenon of spontaneous Ca^{2+} waves and local contraction occurring between paced transients in pressure overload-induced cardiomyopathy. Our observations, enabled by SHG-2PF imaging, raise the possibility that Ca^{2+} sparks and waves increase internal mechanical strain and stress in cardiac myocytes and may therefore contribute to alterations in cellular mechano-chemo-transduction signaling.

METHODS

All laboratory procedures in this study conform to the *Guide for the Care and Use of Laboratory Animals* published by the US National Institutes of Health, the Guide for the Care and Use of Laboratory Animals laid out by Animal Care Committee of the University of California (UC). The animal use was approved by the UC Davis Institutional Animal Care and Use Committee. Please see the Supplementary Materials for cell isolation, dye loading, and antibody labeling protocols.

SHG-2PF imaging

SHG is a process in which light of wavelength λ produces its second harmonic (wavelength ½ λ) as it passes through a noncentrosymmetric medium. The process is coherent, so the medium must have a long-range order and orientation that allows constructive interference of the second harmonic signal. SHG was first demonstrated in noncentrosymmetric crystals,[22] but has since been demonstrated in biological macromolecules, including collagen, tubulin arrays, and sarcomeric myosin.[23–27] SHG occurs strongly when these macromolecules are highly ordered, as they are in tendons, axons, and striated muscle. Because the properties that enable SHG are intrinsic to the macromolecules themselves, exciting and detecting SHG in muscle does not require the use of exogenous or genetic labels; furthermore, SHG is a non-absorptive process and thus is not prone to photobleaching. Several groups have studied SHG in sarcomeric myosin in depth – together, they have shown both the myosin rod and head domains of the thick filaments contribute to the generated signal, while the actin thin filaments do not.[26,28,29] The label-free nature of sarcomeric SHG has been utilized to study sarcomere microarchitecture in muscular dystrophy,[30,31] myofibrilogenesis,[32] and drug-induced myopathy.[33] It has also been developed as a technique to study local actin-myosin cross-bridging[28,29] and *in vivo* contractile dynamics in skeletal muscle.[34] Boulesteix et al. have used it to measure sarcomere length with a reported accuracy of 20-nm in relaxed and tetanic frog cardiac myocytes.[35]

SHG can be readily integrated with two-photon fluorescence (2PF) microscopy. In 2PF, laser light of wavelength λ_{ex} is used to excite an electron transition at energy ½ λ_{ex}. After the loss of vibrational energy, a Stokes-shifted photon is emitted at $\lambda_{em} > ½ \lambda_{ex}$. The shift allows the signal from fluorophores ($\lambda_{em} > ½ \lambda_{ex}$) and harmonophores ($\lambda_{em} = ½ \lambda_{ex}$) to be simultaneously excited, separated, and detected (Figure 1). For our experiments, a Coherent Chameleon outputting 150 femtosecond pulses at a repetition rate of 80 MHz and tuned to a wavelength of 976 nm was used as the excitation source; laser power at the sample was

typically 12 mW. The laser was air-coupled to an Olympus FluoView 300 (FV300) scanning unit with an IX-81 microscope. A 60x/1.2 N.A. water immersion objective was used as the excitation objective. Two-photon excitation at half of the 976 nm wavelength was used to excite Ca^{2+} indicator Fluo-4.

2PF was collected in the epi-direction, separated from the excitation beam with a dichroic mirror, and isolated with a 550 ± 40 nm bandpass filter. SHG was collected in the forward direction with a 50X/0.55 NA extra-long working distance objective and isolated with a 488 ± 10 nm bandpass filter. Emission from SHG and 2PF were simultaneously collected through two separate PMTs. The spatial and temporal resolutions of the SHG-2PF images are defined by the confocal microscope with maximal of x,y~0.25μm, z~0.8μm, t~3μs/pixel. 2-D raster and 1-D line scan images were acquired using the Olympus FluoView software. Post-processing and data analysis were performed using Fiji and Matlab software, and are described below.

RESULTS

Localization of SHG to known contractile and Ca^{2+} handling structures

Previous work has shown that SHG signals from cardiac myocytes originate from the myosin heads of the thick filament and therefore show the position of the A-bands in sarcomere.[25,26] Based on the known ultra-structure, Fig. 2A illustrates the localization of SHG signals in relation to the major structures governing Ca^{2+}-triggered contraction in the sarcomere. We used SHG-2PF imaging to experimentally verify the localization of SHG signals as discussed. In one set of experiments, we immuno-labeled RyRs using antibodies conjugated with Alexa Fluor 488 (AF-488) and subsequently performed multimodal SHG-2PF microscopy as described above. Fig. 2B shows the dual SHG-2PF image so obtained, with punctate RyR staining appearing in sets of A-bands. An enlarged view of a single sarcomere shows that the A-bands and RyR clusters in the SHG-2PF image indeed correspond to the known ultrastructure of cardiac myocytes.

To visualize the localization of SHG signal with respect to the T-tubules, we used Di8-ANEPPS (Di8) to label sarcolemma and T-tubules in live cardiac myocytes. Using a 2-D fast scan, we visualized the entire cardiac myocyte and identified a single myofilament to interrogate further. We then used the confocal linescan mode to obtain fast 1-D SHG-2PF linescans of the myofilament, which are required to capture fast dynamics in live cardiac myocytes. Fig. 2C shows the linescan image acquired by scanning along a single myofilament repetitively. The SHG signal (green) shows the A-bands while the 2PF signal (purple) shows the Di8-labeled T-tubules. In accordance with known ultrastructure and prior microscopy studies, two A-bands are seen within each sarcomere, flanked by a pair of T-tubules. The fluorescence intensity profiles (bottom panel) allow the quantifying of the position and distance between these SHG-2PF signals.

Simultaneous imaging of the A-band and Ca^{2+} at high spatial and temporal resolution

To image Ca^{2+}-contraction coupling, we loaded freshly isolated cardiac myocytes with the fluorescent Ca^{2+} indicator Fluo-4. Figure 3 shows a sample SHG-2PF linescan image

acquired at a spatial resolution of 1024 pixels per line, and a temporal resolution of 9.3 ms per line (9.1 μs/pixel). A Ca^{2+} transient is seen in the increase of Fluo-4 fluorescence (Fig. 3A, left) and the triggered sarcomere contraction is seen from the displacement of the SHG signals (Fig. 3A, right). Subsequent linescans were obtained at faster speeds of 3.1 ms per line (~3.1 μs/pixel).

To resolve sarcomere contraction from the SHG signals, we calculated the distance between adjacent A-bands. As illustrated in Fig. 3B, we denote L_M as the distance between the two A-bands within the same sarcomere (seen between the T-tubules, traversing the M-line), and L_Z as the distance between the adjacent A-bands across the sarcomere (seen across the T-tubule, traversing the Z-line). L_M and L_Z each can be measured from the distance between the adjacent SHG bright bands. During contraction, L_Z is shortened by increased overlap of the thick and thin filaments, while the L_M remains unchanged because the length of the thick filament within a sarcomere does not change. The sum of L_M and L_Z is equal to the sarcomere length, $L_{SL} = L_M + L_Z$ (e.g. the distance from Z-line to Z-line, or equivalently from M-line-to-M-line).

We used the above definitions to measure L_M and L_Z from the distance between the SHG bright bands in Fig. 3C. The histogram of inter-A-band distances can be calculated using the kernel density method (see Online Methods).[36,37] During diastole (green framed region, Fig. 3A), the histogram of distances between adjacent A-bands shows two distinct peaks (green curves, Fig. 3C), corresponding to L_M~0.8μm and L_Z~1.0μm. During systole (red framed region, Fig. 3A), the histogram also shows two peaks (red curves, Fig. 3C), but corresponding to L_M~0.8μm and L_Z~0.9μm. Thus, in agreement with our analysis, L_M is constant and L_Z is shortened during contraction. The calculated sarcomere lengths $L_{SL} = L_M + L_Z$ in these states are L_{SL}~1.8μm at diastole (the slack length in an isolated cardiac myocyte) and L_{SL}~1.6μm at systole. To verify the sarcomere length values calculated using the SHG image, we also directly measured the sarcomere length from the transmission image of the myocyte using an established method (Online Fig. I). We obtained a sarcomere length of 1.8 μm at diastole and 1.6 μm at systole, in agreement with the values calculated from the SHG image.

Construction of strain maps of sarcomere contraction from SHG image analysis

We developed an automated image analysis method to extract local sarcomere contraction information from the SHG linescan images. Figure 4 depicts the analysis procedure. First, we reduced the noise in the raw SHG image data by applying a 2-D Wiener filter (Fig. 4B). The Wiener filter requires the neighborhood size of the relevant image features to be defined. In the SHG linescan image, the neighborhood in space is set to roughly one-half of the width of the more narrow SHG-dark bands (which corresponds to the M-line positions). The neighborhood in time is set according to the speed and magnitude of contractions that are present in the data (e.g. if the contractions are rapid and involve significant translation, a small time neighborhood is chosen). Second, after noise reduction, a 2-D Fast Fourier Transform (FFT) of the spatial SHG signal is performed line-by-line, and then each FFT is bandpass filtered (Fig. 4C). The band that is retained corresponds to spatial periods of 300 nm to 2.5 μm and contains the key spatial frequencies and phases of the A-band signal. Each

line is then inverse Fourier transformed to obtain a smooth, oscillating signal that is in phase with the SHG-bright bands (Fig. 4D). Third, from this signal the minima between SHG-bright bands are obtained (red lines in Fig. 4E), which are used to set processing windows around the SHG-bright bands. Gaussian fitting is then employed to estimate the center of each SHG-bright band at each point in time. The results of Gaussian fitting (yellow lines in Fig. 4F) therefore estimate the center of the A-bands. The distance between the center of the A-bands corresponds to the L_M and L_Z peaks as discussed previously. Histograms of the center-to-center distances during diastole and systole show that myocyte contraction shortens L_Z while L_M remains unchanged (Fig. 4G and 4H, and Online Fig. II). Thus our automated analysis is able to extract expected changes in the distances between adjacent A-bands.

Next, we construct a strain map that displays sarcomere contraction and relaxation through time by using the centers of the SHG-bright bands. We first use a moving local linear regression to smooth the data through time (Online Figs. III and IV). The strain over a given sarcomeric distance is then calculated as $E = (L\ L_0)/L_0$, where L is the distance between a SHG-bright band and its next nearest neighbor, and L_0 is that distance averaged over the first 25 pixels in time (when the cell is relaxed). Fig. 5 (middle panels) show sample strain maps computed from the SHG-2PF images obtained from cardiac myocytes at different contractile states.

Correlation between Ca^{2+} and strain maps in cardiac myocytes at different contractile states

To investigate local Ca^{2+}-contraction coupling, we plotted the strain map and Ca^{2+} image side-by-side in Fig. 5. Fig. 5A shows a relaxed state with no development of strain (left and mid panels) at low resting Ca^{2+} concentration (right panel). Fig. 5B shows a development of strain across sarcomeres (left and mid panels) in response to a propagating Ca^{2+} wave (right panel). Higher strain correlates to higher Ca^{2+} in space, and a time lag between Ca^{2+} rise and strain development can be observed. Fig. 6A demonstrates that the normalized cross-correlation between the strain and the corresponding Ca^{2+} signal ranges from 0.90 to 0.93 for the sarcomere “lanes” seen in Fig. 5B (mean = 0.92, $\sigma = 0.01$); the time delay to the cross correlation maximum ranges from 114.7 ms to 192.2 ms (mean = 149.3 ms, $\sigma = 30.3$ ms). These delays are in agreement with the observation at the whole cell level that there is a lag between the Ca^{2+} transient and cardiac myocyte contraction.[38] Thus, multi-modal SHG-2PF microscopy is capable of capturing the sequential development of strain in individual sarcomeres in response to a propagating Ca^{2+} wave.

The method also enables us to answer a previously unresolved question: do Ca^{2+} sparks cause local sarcomere contraction? To analyze the correlation between Ca^{2+} sparks and the nearest neighbor A-bands, we computed the strain map from M-line to M-line (Fig. 5C, mid panel). Fig. 5C shows the development of microdomain strain (mid panel) in response to localized Ca^{2+} sparks (right panel). A positive correlation between Ca^{2+} sparks and local strain can be observed, although the time delay for strain development is variable (addressed below). Thus, Ca^{2+} sparks can indeed cause local sarcomere contractions (termed *myo-pinch*) that lead to non-uniform strain in subcellular microdomains.

In Fig. 6C, events from Fig. 5C with an apparent spark-strain correlation (Fig. 6B) are plotted separately. In these plots, history dependence can be observed: peak strain develops earlier for sparks that occur shortly after a prior spark-strain event (Fig. 6C, plots 1, 2, 4, and 5: avg. time to peak strain = 176.2 ms) than for those with a longer strain-free history (Fig. 6C, plots 3, 7, and 8: avg. time to peak strain = 75.4 ms). Some of the Ca^{2+} spark-induced myo-pinches are small in magnitude; we excluded those that are outside of our 85% confidence intervals on strain (Online Fig. V). Additionally, we examined the effect of our smoothing algorithm on Ca^{2+} spark-induced myo-pinch as well as on simulated strain and confirmed that smoothing does not attenuate strain events that lasts for 60 ms or longer (Online Figs. VI and VII); myo-pinch events lasted > 100 ms in our observations.

Ca^{2+} -contraction coupling in a murine model of pressure-overload induced cardiomyopathy

To demonstrate the utility of the SHG-2PF imaging modality in disease model animals, we used transverse aortic constriction (TAC) surgery to generate pressure-overload mice who develop cardiac hypertrophy and heart failure [39] (online methods). cardiac myocytes from TAC mice were studied under mechanical load using the “cell-in-gel” system as previously described,[40] as well as under standard load-free conditions. When load-free, TAC cardiac myocytes responded to electrical pacing with regular contractions (Fig. 7A). Under mechanical load, however, the cells displayed aberrant spontaneous Ca^{2+} waves at variable times during diastole, between paced systolic Ca^{2+} transients (Fig. 7B). Fig. 7C–E show a strain map analysis of one such aberrant Ca^{2+} wave, amongst paced transients, in a TAC cardiac myocyte under mechanical load. Panel C shows the SHG data, panel D shows the strain map obtained from an analysis of two adjacent sarcomeres, and panel E shows the corresponding 2PF data. At the single-sarcomere level (Fig. 7F–G), the wave-triggered contractions were lower in amplitude than the paced contractions. Consistently, the amplitude of the contractions correlated to the relative change in intra-sarcomere calcium levels. These results demonstrate the applicability of the SHG-2PF technique to study of mechanical stress-induced heart disease.

DISCUSSION

Imaging local Ca^{2+}-contraction coupling at sarcomere resolution in cardiac myocytes is difficult with available techniques yet necessary for investigating the molecular mechanisms that link mechanical stress to heart diseases. In this project, we developed a multimodal SHG-2PF technique to image Ca^{2+}-induced strain at the single sarcomere level. The technique utilized a single laser to excite SHG from the thick filaments of sarcomeres and 2PF from a fluorescent Ca^{2+} indicator, simultaneously. First, we developed the methods and algorithms for acquiring, processing, and interpreting the multimodal image data. Second, we verified the SHG analysis by comparing the SHG signal to the known ultrastructure of sarcomere and the Ca^{2+} handling molecules (i.e. A-band, T-tubule, and RyRs). Third, we tested the feasibility of using the SHG-2PF technique to simultaneously image Ca^{2+} and sarcomere contractions. We were able to make the novel observation in live cardiac myocytes that Ca^{2+} sparks can induce local mechanical strain at the sarcomere level, a phenomenon we named myo-pinch. Finally, we applied the technique to a murine model of

mechanical stress-induced heart disease; when these cardiac myocytes were placed under mechanical load, we observed calcium waves and associated sarcomere strain occurring between paced transients.

Multimodal SHG-2PF imaging has distinct advantages over other available techniques. Recently Shintani et al. developed a method for measuring sarcomere shortening by labeling the Z-discs with AcGFP-tagged α-actinin for imaging.[15] However, the method uses vector-mediated transfection of cardiac myocytes that requires culturing the cells to express adequate amount of AcGFP-tagged α-actinin. In culture, both neonatal and adult cardiac myocytes undergo changes in the Ca^{2+} handling and contractile characteristics[41–43], and hence may introduce artifacts. Genetic labeling methods are also disadvantaged by potential interference between GFP and sarcomeric protein function.[18] In contrast, we use SHG to accomplish label-free and non-invasive imaging of A-bands within the sarcomeres of live cardiac myocytes.

Another sarcomere-tracking technique utilizes labeled T-tubules. However, T-tubules in cardiac myocytes, even those from the healthy hearts, display a significant variance in the regularity, direction, diameter and distance from Z-discs.[44] In some disease states such as hypertrophy and heart failure, T-tubule networks can become irregular and 'detubulated'.[45,46] In comparison, SHG is intrinsic to the thick filaments of sarcomere and is detectable as long as the sarcomeres remain intact. Therefore, SHG microscopy is ideally suited for studying sarcomere-level contraction in heart disease models.

Both genetic labeling and T-tubule labeling are further restrictive when used in conjunction with fluorescent Ca^{2+} indicators for dual imaging. The fluorophores must be carefully selected for each imaging modality in accordance with the kinetics of the indicator and to allow spectral separation. It may not be possible to minimize the crosstalk between sarcomere markers such as GFP and fluorescent Ca^{2+} indicators such as Fluo-4. The use of SHG circumvents this difficulty because SHG has a signal wavelength of $\lambda_{ex}/2$; any fluorescent label used for 2PF will be Stokes-shifted and separable from the second harmonic signal. Therefore, SHG provides a superb add-on modality for simultaneously imaging sarcomere contraction with Ca^{2+} signals.

The multimodal method as presented enabled us to show that Ca^{2+} sparks can cause local sarcomere contractions. However, it can be further refined to increase the signal-to-noise (S/N) ratio and improve the quantification of small contraction events. One way to address this is to raise the laser power. In our preliminary experiments, however, higher laser powers than what were used caused some degree of laser-induced Ca^{2+} release and photon damage, and therefore limited the achievable S/N ratio for SHG. For future improvements, several approaches can increase the S/N ratio in multiphoton microscopes. For example, our OEM-installed fiber bundle that collects forward-directed light does not collect 100% of the photons; bypassing the fiber and collecting SHG photons directly using a photon multiplier tube (PMT) would double the SHG signal.[47,48] Compressing the femtosecond laser pulses used to excite SHG and 2PF by chirping can significantly improve S/N ratio in multiphoton processes, because generated signals scale quadratically with the peak power of the pulse.[49]

These approaches can be combined to improve the S/N ratio and therefore our ability to estimate the center of mass of the A-bands.

A potential limitation of the SHG-2PF method lies in measuring strain during global (e.g. electrically stimulated) contractions in load-free cardiac myocytes, if the motion is too large to keep the same sarcomere within the focus of the confocal microscope. Due to the highly localized nature of the SHG-2PF technique, it is best used to track local sarcomere contraction in response to local Ca^{2+} releases. For the measurement of global contractions, however, there are a number of established methods (edge detection, sarcomere pattern measurement using FFT, etc.). The main advantage of the technique we developed here is that it allows one to “zoom in” and measure microdomain contraction -- morphological changes in A-bands within individual sarcomeres -- in response to local Ca^{2+} signals.

Super resolution microscopy is a rapidly evolving field and may impact SHG-2PF imaging in the future. A-bands are readily resolvable with our current technique, but any improvement in resolution will improve precision in the determination of A-band centers. Though no super resolution method currently exists for harmonic generation microscopy, several investigators are actively developing label-free super resolution methods.[50,51] As a special consideration to Ca^{2+} imaging, the usefulness of super resolution methods is limited by the fact that Ca^{2+} diffuses rapidly and small molecule Ca^{2+} indicators also have limited on/off kinetics. A promising approach may be to express localized Ca^{2+} indicators[52–55] in subcellular compartments to further quantify local Ca^{2+} levels in relation to sarcomere strain.

In summary, we have developed multimodal SHG-2PF imaging as a new, enabling tool for simultaneously imaging Ca^{2+} levels and sarcomere contraction in live cardiac myocytes with confocal resolution. Our method permits the investigation of the relationship between localized Ca^{2+} release events and mechanical strain in subcellular microdomains. Such knowledge is important for understanding the mechano-chemo-transduction within the cell that contributes to mechanical stress-induced heart diseases.

Supplementary Material

Refer to Web version on PubMed Central for supplementary material.

Acknowledgments

S.A. would like to thank the California Institute of Regenerative Medicine’s Stem Cell Training Program at UC Davis and the UC Davis Physician-Scientist Training Program for graduate student scholarships.

SOURCES OF FUNDING

This work is supported by a UC Davis Academic Senate Faculty Research Grant to JWC and YC, National Institute of Health NIH R01HL90880 to LTI and YC, NIH R01HL123526 to YC, R03AG031944 to YC, R01HL85844 and HL85727 to NC, NSF 1264776 to JWC and DKL, and by the Center for Biophotonics, National Science Foundation Science and Technology Center that is managed by the University of California, Davis, under cooperative agreement No. PHY 0120999. This work is also supported, in part, by the University of California startup funds to YC.

Nonstandard Abbreviations and Acronyms

SHG	Second harmonic generation
2PF	Two-photon fluorescence
SR	Sarcoplasmic reticulum
RyR	Ryanodine receptor
CICR	Calcium-induced calcium release
CRU	Calcium release unit
FFT	Fast Fourier transform

References

1. Bers, DM. Excitation-Contraction Coupling and Cardiac Contractile Force. 2. Dordrecht: Kluwer Academic Publishers; 2001.
2. Chen-Izu Y, McCulle SL, Ward CW, et al. Three-dimensional distribution of ryanodine receptor clusters in cardiac myocytes. Biophys J. 2006; 91:1–13. [PubMed: 16603500]
3. Soeller C, Jayasinghe ID, Li P, Holden AV, Cannell MB. Three-dimensional high-resolution imaging of cardiac proteins to construct models of intracellular Ca2+ signalling in rat ventricular myocytes. Exp Physiol. 2009; 94:496–508. [PubMed: 19139064]
4. Cheng H, Lederer WJ, Cannell MB. Calcium Sparks: Events Underlying Elementary Excitation-Contraction Coupling in Heart Muscle. Science. 1993; 262:740–744. [PubMed: 8235594]
5. Cannell MB, Cheng H, Lederer WJ. Spatial Non-Uniformities in [Ca2+]i during Excitation-Contraction Coupling in Cardiac Myocytes. Biophys J. 1994; 67:1942–1956. [PubMed: 7858131]
6. López-López JR, Shacklock PS, Balke CW, Wier WG. Local, stochastic release of Ca2+ in voltage-clamped rat heart cells: visualization with confocal microscopy. J Physiol. 1994; 480(1):21–29. [PubMed: 7853223]
7. Boyden, Pa; Pu, J.; Pinto, J.; Keurs, HEDJT. Ca2+ Transients and Ca2+ Waves in Purkinje Cells: Role in Action Potential Initiation. Circ Res. 2000; 86:448–455. [PubMed: 10700450]
8. Schlotthauer K, Bers DM. Sarcoplasmic Reticulum Ca2+ Release Causes Myocyte Depolarization: Underlying Mechanism and Threshold for Triggered Action Potentials. Circ Res. 2000; 87:774–780. [PubMed: 11055981]
9. Berlin JR, Cannell MB, Lederer WJ. Cellular origins of the transient inward current in cardiac myocytes. Role of fluctuations and waves of elevated intracellular calcium. Circ Res. 1989; 65:115–126. [PubMed: 2736729]
10. Bers DM. Cardiac sarcoplasmic reticulum calcium leak: basis and roles in cardiac dysfunction. Annu Rev Physiol. 2014; 76:107–127. [PubMed: 24245942]
11. Chengh H, Lederer WJ. Calcium Sparks. Physiol Rev. 2008; 88:1491–1545. [PubMed: 18923188]
12. Balligand J, Feron O, Dessy C. eNOS Activation by Physical Forces: From Short-Term Regulation of Contraction to Chronic Remodeling of Cardiovascular Tissues. Physiol Rev. 2009; 89:481–534. [PubMed: 19342613]
13. Bub G, Camelliti P, Bollensdorff C, et al. Measurement and analysis of sarcomere length in rat cardiac myocytes in situ and in vitro. Am J Physiol Heart Circ Physiol. 2010; 298:H1616–H1625. [PubMed: 20228259]
14. Serizawa T, Terui T, Kagemoto T, et al. Real-time measurement of the length of a single sarcomere in rat ventricular myocytes: a novel analysis with quantum dots. Am J Physiol Cell Physiol. 2011; 301:C1116–C1127. [PubMed: 21813712]
15. Shintani, Sa; Oyama, K.; Kobirumaki-Shimozawa, F.; Ohki, T.; Ishiwata, S.; Fukuda, N. Sarcomere length nanometry in rat neonatal cardiac myocytes expressed with α-actinin-AcGFP in Z discs. J Gen Physiol. 2014; 143:513–524. [PubMed: 24638993]

16. Louch WE, Bito V, Heinzel FR, et al. Reduced synchrony of Ca2+ release with loss of T-tubules-a comparison to Ca2+ release in human failing cardiac myocytes. Cardiovasc Res. 2004; 62:63–73. [PubMed: 15023553]
17. Lyon AR, MacLeod KT, Zhang Y, et al. Loss of T-tubules and other changes to surface topography in ventricular myocytes from failing human and rat heart. Proc Natl Acad Sci U S A. 2009; 106:6854–6859. [PubMed: 19342485]
18. Agbulut O, Huet A, Niederländer N, Puceat M, Menasché P, Coirault C. Green fluorescent protein impairs actin-myosin interactions by binding to the actin-binding site of myosin. J Biol Chem. 2007; 282:10465–10471. [PubMed: 17289667]
19. Sekar RB, Kizana E, Smith RR, Barth AS, Zhang Y, Tung L. Lentiviral vector-mediated expression of GFP or Kir2. 1 alters the electrophysiology of neonatal rat ventricular myocytes without inducing cytotoxicity. Am J Physiol Heart Circ Physiol. 2007; 21205:2757–2770.
20. Nishimura S, Nagai S, Sata M, et al. Expression of green fluorescent protein impairs the force-generating ability of isolated rat ventricular cardiac myocytes. Mol Cell Biochem. 2006; 286:59–65. [PubMed: 16532258]
21. Telley I. Half-sarcomere dynamics in myofibrils during activation and relaxation studied by tracking fluorescent markers. Biophys J. 2006; 90:514–530. [PubMed: 16239326]
22. Franken PA, Hill AE, Peters CW, Weinreich G. Generation of opical harmonics. Phys Rev Lett. 1961; 7:118–119.
23. Fine S, Hansen WP. Optical second harmonic generation in biological systems. Appl Opt. 1971; 10:2350–2353. [PubMed: 20111328]
24. Guo Y, Ho PP, Tirksliunas A, Liu F, Alfano RR. Optical harmonic generation from animal tissues by the use of picosecond and femtosecond laser pulses. Appl Opt. 1996; 35:6810–6813. [PubMed: 21151266]
25. Campagnola PJ, Millard AC, Terasaki M, Hoppe PE, Malone CJ, Mohler WA. Three-dimensional high-resolution second-harmonic generation imaging of endogenous structural proteins in biological tissues. Biophys J. 2002; 81:493–508. [PubMed: 11751336]
26. Plotnikov SV, Millard AC, Campagnola PJ, Mohler WA. Characterization of the myosin-based source for second-harmonic generation from muscle sarcomeres. Biophys J. 2006; 90:693–703. [PubMed: 16258040]
27. Dombeck, Da; Kasischke, Ka; Vishwasrao, HD.; Ingelsson, M.; Hyman, BT.; Webb, WW. Uniform polarity microtubule assemblies imaged in native brain tissue by second-harmonic generation microscopy. Proc Natl Acad Sci U S A. 2003; 100:7081–7086. [PubMed: 12766225]
28. Nucciotti V, Stringari C, Sacconi L, et al. Probing myosin structural conformation in vivo by second-harmonic generation microscopy. Proc Natl Acad Sci U S A. 2010; 107:7763–7768. [PubMed: 20385845]
29. Schürmann S, von Wegner F, Fink RHa, Friedrich O, Vogel M. Second harmonic generation microscopy probes different states of motor protein interaction in myofibrils. Biophys J. 2010; 99:1842–1851. [PubMed: 20858429]
30. Plotnikov SV, Kenny AM, Walsh SJ, et al. Measurement of muscle disease by quantitative second-harmonic generation imaging. J Biomed Opt. 2008; 13:044018. [PubMed: 19021346]
31. Friedrich O, Both M, Weber C, et al. Microarchitecture is severely compromised but motor protein function is preserved in dystrophic mdx skeletal muscle. Biophys J. 2010; 98:606–616. [PubMed: 20159157]
32. Liu H, Shao Y, Qin W, et al. Myosin filament assembly onto myofibrils in live neonatal cardiac myocytes observed by TPEF-SHG microscopy. Cardiovasc Res. Nov.2012 :262–270. [PubMed: 23118131]
33. Huang S-H, Hsiao C-D, Lin D-S, Chow C-Y, Chang C-J, Liau I. Imaging of zebrafish in vivo with second-harmonic generation reveals shortened sarcomeres associated with myopathy induced by statin. PLoS One. 2011; 6:e24764. [PubMed: 21966365]
34. Llewellyn ME, Barretto RPJ, Delp SL, Schnitzer MJ. Minimally invasive high-speed imaging of sarcomere contractile dynamics in mice and humans. Nature. 2008; 454:784–788. [PubMed: 18600262]

35. Boulesteix T, Beaurepaire E, Sauviat M-P, Schanne-Klein M-C. Second-harmonic microscopy of unstained living cardiac myocytes: measurements of sarcomere length with 20-nm accuracy. Opt Lett. 2004; 29:2031–2033. [PubMed: 15455770]
36. Scott DW, Tapia RA, Thompson JR. Kernel density estimation revisited. Nonlinear Anal Theory, Methods Appl. 1977; 1:339–372.
37. Silverman, BW. Density Estimation for Statistics and Data Analysis. Boca Raton, FL: Chapman and Hall; 1986.
38. Bers DM. Cardiac excitation-contraction coupling. Nature. 2002; 415:198–205. [PubMed: 11805843]
39. Rockman HA, Ross RS, Harris AN, et al. Segregation of atrial-specific and inducible expression of an atrial natriuretic factor transgene in an in vivo murine model of cardiac hypertrophy. Proc Natl Acad Sci. 1991; 88:8277–8281. [PubMed: 1832775]
40. Jian Z, Han H, Zhang T, et al. Mechanochemotransduction during cardiac myocyte contraction is mediated by localized nitric oxide signaling. Sci Signal. 2014; 7:ra27. [PubMed: 24643800]
41. Husse B, Wussling M. Developmental changes of calcium transients and contractility during the cultivation of rat neonatal cardiac myocytes. Mol Cell Biochem. 1996; 163/164:13–21. [PubMed: 8974035]
42. Kostin S, Hein S, Bauer EP, Schaper J. Spatiotemporal Development and Distribution of Intercellular Junctions in Adult Rat cardiac myocytes in Culture. Circ Res. 1999; 85:154–167. [PubMed: 10417397]
43. Hersch N, Wolters B, Dreissen G, et al. The constant beat: cardiac myocytes adapt their forces by equal contraction upon environmental stiffening. Biol Open. 2013; 2:351–361. [PubMed: 23519595]
44. Soeller C, Cannell MB. Examination of the Transverse Tubular System in Living Cardiac Rat Myocytes by 2-Photon Microscopy and Digital Image Processing Techniques. Circ Res. 1999; 84:266–275. [PubMed: 10024300]
45. Heinzel FR, Bito V, Biesmans L, et al. Remodeling of T-tubules and reduced synchrony of Ca2+ release in myocytes from chronically ischemic myocardium. Circ Res. 2008; 102:338–346. [PubMed: 18079411]
46. Dibb KM, Clarke JD, Horn Ma, et al. Characterization of an extensive transverse tubular network in sheep atrial myocytes and its depletion in heart failure. Circ Heart Fail. 2009; 2:482–489. [PubMed: 19808379]
47. Majewska A, Yiu G, Yuste R. A custom-made two-photon microscope and deconvolution system. Eur J Physiol. 2000; 441:398–408.
48. Nikolenko V, Nemet B, Yuste R. A two-photon and second-harmonic microscope. Methods. 2003; 30:3–15. [PubMed: 12695099]
49. Xi P, Andegeko Y, Pestov D, Lovozoy VV, Dantus M. Two-photon imaging using adaptive phase compensated ultrashort laser pulses. J Biomed Opt. 2013; 14:014002. [PubMed: 19256690]
50. Chowdhury S, Izatt J. Structured illumination diffraction phase microscopy for broadband, subdiffraction resolution, quantitative phase imaging. Opt Lett. 2014; 39:1015–1018. [PubMed: 24562266]
51. Wang P, Slipchenko MN, Mitchell J, Yang C, Potma EO, Xu X. Far-field imaging of non-fluorescent species with subdiffraction resolution. Nat Photonics. 2013; 7:449–453. [PubMed: 24436725]
52. Kaestner L, Scholz A, Tian Q, et al. Genetically encoded Ca2+ indicators in cardiac myocytes. Circ Res. 2014; 114:1623–1639. [PubMed: 24812351]
53. Shang W, Lu F, Sun T, et al. Imaging Ca2+ nanosparks in heart with a new targeted biosensor. Circ Res. 2014; 114:412–420. [PubMed: 24257462]
54. Luo X, Hill Ja. Ca^{2+} in the cleft: fast and fluorescent. Circ Res. 2014; 115:326–328. [PubMed: 25035130]
55. Zhao Y-T, Valdivia HH. Ca2+ nanosparks: shining light on the dyadic cleft but missing the intensity of its signal. Circ Res. 2014; 114:396–398. [PubMed: 24481836]

Novelty and Significance

What Is Known?

- Global Ca^{2+} release from the intracellular Ca^{2+} store causes cardiac myocyte contraction.
- Localized Ca^{2+} release such as Ca^{2+} sparks often occur in diseased hearts, but whether the Ca^{2+} spark can cause local sarcomere contraction was unresolved due to a lack of suitable technique.

What New Information Does This Article Contribute?

- We developed a multimodal SHG-2PF (second harmonic generation and two-photon fluorescence) microscopy technique to simultaneously image the local Ca^{2+} signal and sarcomere contraction at high spatiotemporal resolution.
- Our data show that Ca^{2+} sparks can cause sarcomere contraction in subcellular microdomains (named myo-pinch), revealing a role for these events in generating subcellular strain during diastole.
- Local Ca^{2+}-contraction coupling is found altered in pressure-overload induced heart failure; such changes in heart diseases can be studied by using the multimodal technique.

During the cardiac cycle, cardiac myocytes contract in systole to pump blood and relax in diastole to allow refilling. Systolic contraction is caused by a global release of Ca^{2+} from the sarcoplasmic reticulum (SR) to increase cytosolic Ca^{2+} concentration. Diastolic relaxation requires Ca^{2+} to be sequestered into the SR and the cytosolic Ca^{2+} concentration to be kept low. However, spontaneous Ca^{2+} release from the SR can occur during diastole, especially in diseased hearts. Whether localized Ca^{2+} release, in the form of Ca^{2+} sparks, can cause local sarcomere contraction has been an important but unresolved issue.

Here we develop a multimodal SHG-2PF imaging method that uses SHG to monitor the contraction of individual sarcomeres and 2PF to image a fluorescent Ca^{2+} indicator. This enables the simultaneous imaging of local Ca^{2+} signals and sarcomere contraction at high spatiotemporal resolution. Our data reveal that Ca^{2+} sparks can indeed cause sarcomere contractions in subcellular microdomains, which suggests that they increase mechanical stress within the cell during diastole. We also find that microdomain Ca^{2+}-contraction coupling is altered in pressure-overload induced heart failure. Thus, the SHG-2PF technique enables the deciphering of disease related changes in Ca^{2+}-contraction coupling at the single sarcomere level.

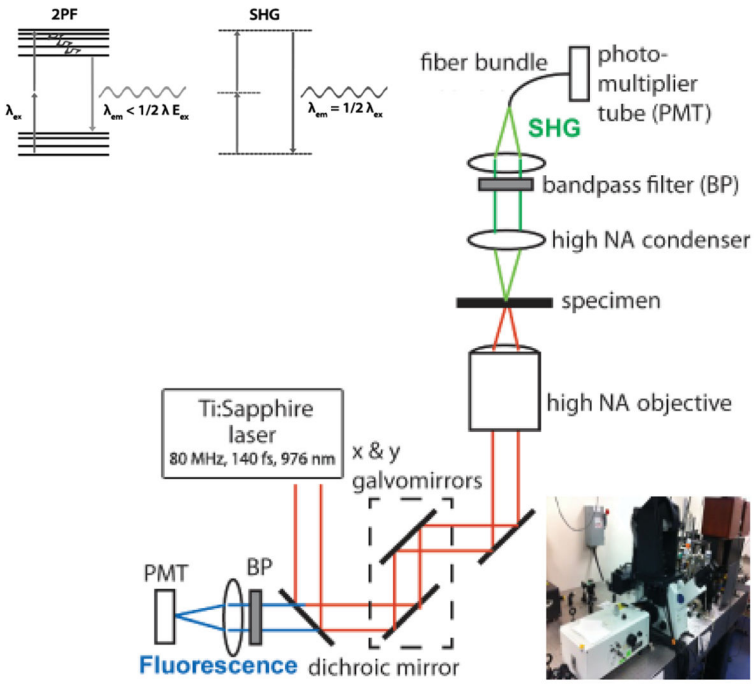

Figure 1. Basics of multimodal SHG-2PF imaging

Jablonski diagrams help distinguish SHG and 2PF. Two photons excite a transition between states in both processes; the states are virtual in SHG and real in 2PF. Vibration reduces the energy of the excited state before 2PF emission. In contrast, no relaxation occurs with SHG. The schematic of our setup, detailed in the text, is depicted above.

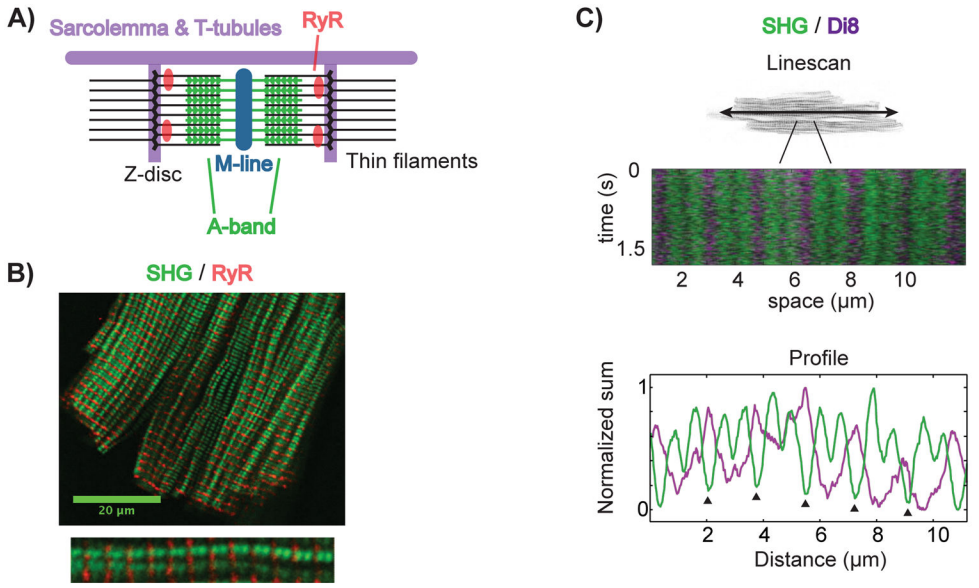

Figure 2. SHG localizes to the thick filaments of sarcomeres

SHG originates from the thick filaments of sarcomeres. RyRs reside on the sarcoplasmic reticulum, adjacent to Z-discs. TTs course along myofilaments and wrap around Z-discs. (A) depicts the localization of these structures to sarcomeric SHG. (B) SHG (green)-2PF (red) imaging of a rVCM immunostained using anti-RYR2-AF488 antibodies, with a single myofilament enlarged below. (C) A multimodal line scan along a single myofilament in a live rVCM loaded with Di-8-ANEPPS. Below is a plot of the signals summed in time, showing the double-banding pattern of sarcomeric SHG with deeper minima (arrowheads) corresponding Z-disc locations.

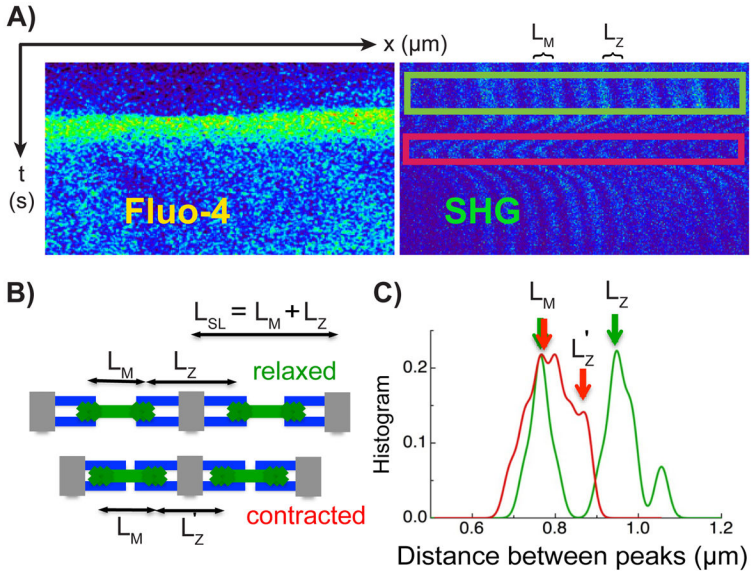

Figure 3. Relationship between sarcomere structure and A-band position

(A) SHG-2PF linescan imaging of the myocyte shows a Ca^{2+} transient seen in the Fluo-4 signal (top left panel of images on right) and the triggered contraction in the SHG signal (top right panel). (B) L_M is the distance between two adjacent A-bands within the same sarcomere. L_Z is the distance between the two A-bands across the adjacent sarcomeres. The sarcomere length L_{SL} is equal to the sum of L_M and L_Z. L_Z shortens during cell contraction due to the sliding of the thick filament against the thin filament. (C) The histogram of A-bands distances is calculated using the kernel density method described in the online methods. L_M is determined by the thick filament structure within the sarcomere and does not change during cell contraction. L_Z shortens as described. The numerical values of L_{SL} during systole and diastole calculated in this way match with sarcomere length calculated using a Fourier transform based method in a similar myocyte (Online Figure I).

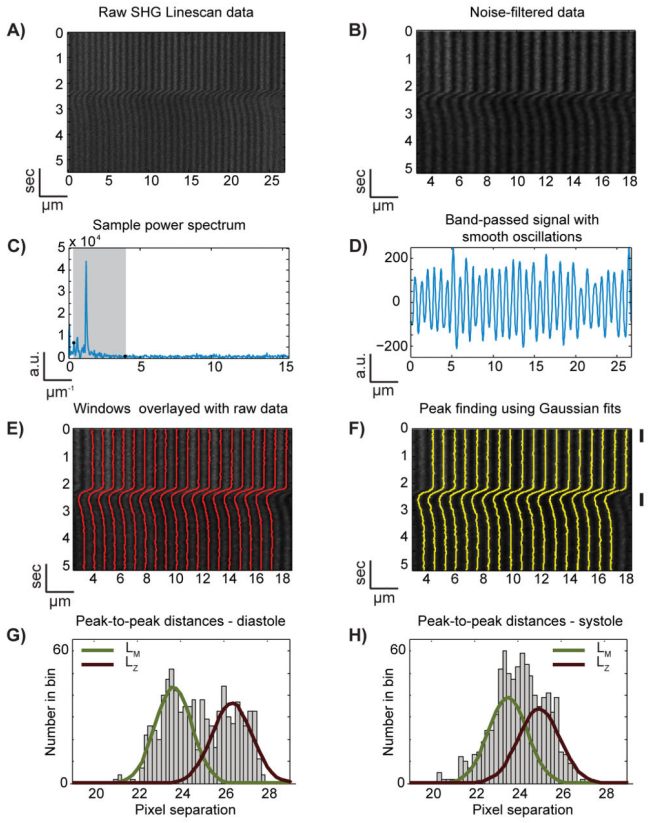

Figure 4. The centers of SHG-bright bands can be identified at each time point

In order to track the peaks of the SHG bands in the raw data (A), noise filtered data (B) is Fourier transformed and bandpass-filtered (C) in order to obtain a smoothly varying signal (D) from which windows for peak fitting can be readily defined (E). Next, each SHG band is fit with a Gaussian at each point in time to determine the center of each SHG band (F). These centers are then used for further analysis. Histograms of the center-to-center distances during diastole (G, corresponding to time frame indicated by the upper-most black bar to the right of F) and systole (H, bottom black bar of F) show that L_M does not change during contraction, whereas L_Z shortens, as expected from Fig. 3. The displayed Gaussian fits of the histogram data come from fitting single Gaussian functions to the L_M and L_Z data separately (Online Figure II).

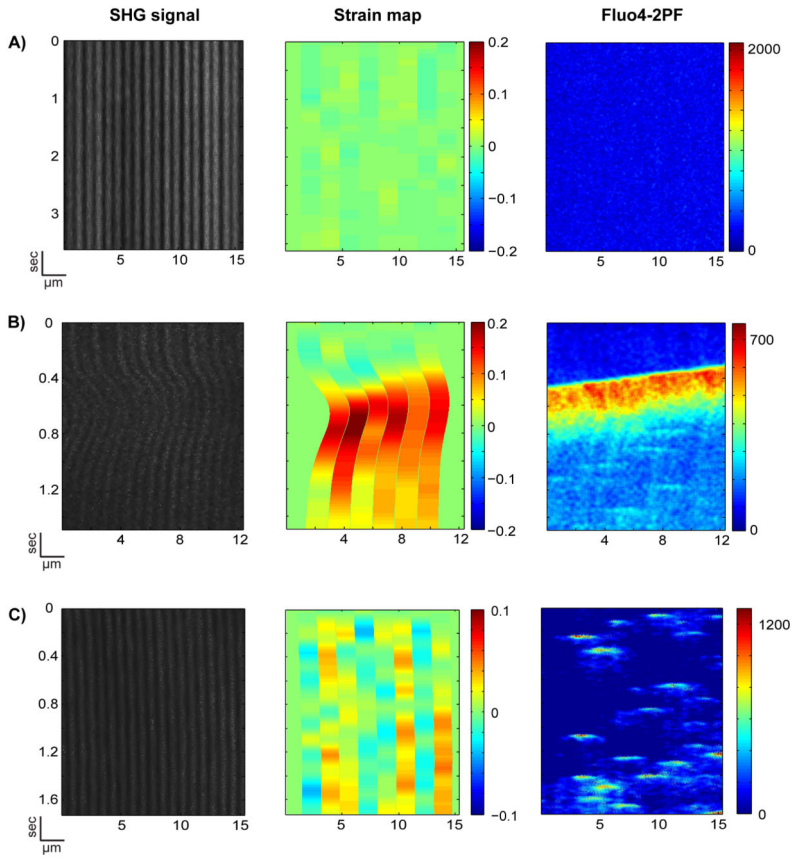

Figure 5. Strain maps constructed from SHG-bright bands demonstrate local calcium-correlated contraction

Strain across a sarcomere length is calculated using the distance between every other SHG-bright band, L, and the average of that distance for the first 25 pixels in time, L_0. Strain is $(L-L_0)/L_0$. In AC, the left images show the noise-filtered raw data. On the right are the simultaneously obtained 2PF signals from Fluo-4-AM. (A) shows a negative control – a rat VCM at resting state. (B) shows a contraction in which transient non-uniform strain develops in response to a calcium wave. (C) shows a strain map, interpolated onto an M-line to M-line grid, resulting from calcium sparks. The area of zero strain on either side of each strain map is an edge artifact; strain was not calculated in these regions.

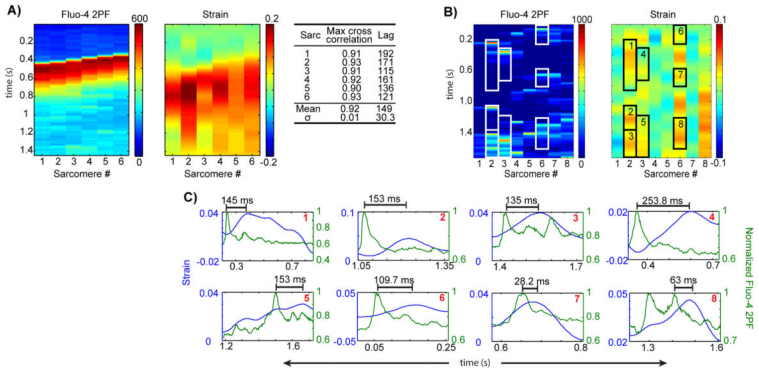

Figure 6. Deeper analysis of sarcomere-scale calcium-contraction coupling

(A) Average Fluo-4 2PF across distances over which strain was calculated, for a calcium wave, next to strain. Table: the normalized cross-correlations between 2PF and strain for each lane. (B) Average Fluo-4-2PF across distances over which strain was calculated, next to strain, during calcium sparks. Myo-pinch phenomena that lie within 85% confidence intervals are boxed and plotted individually in (C).

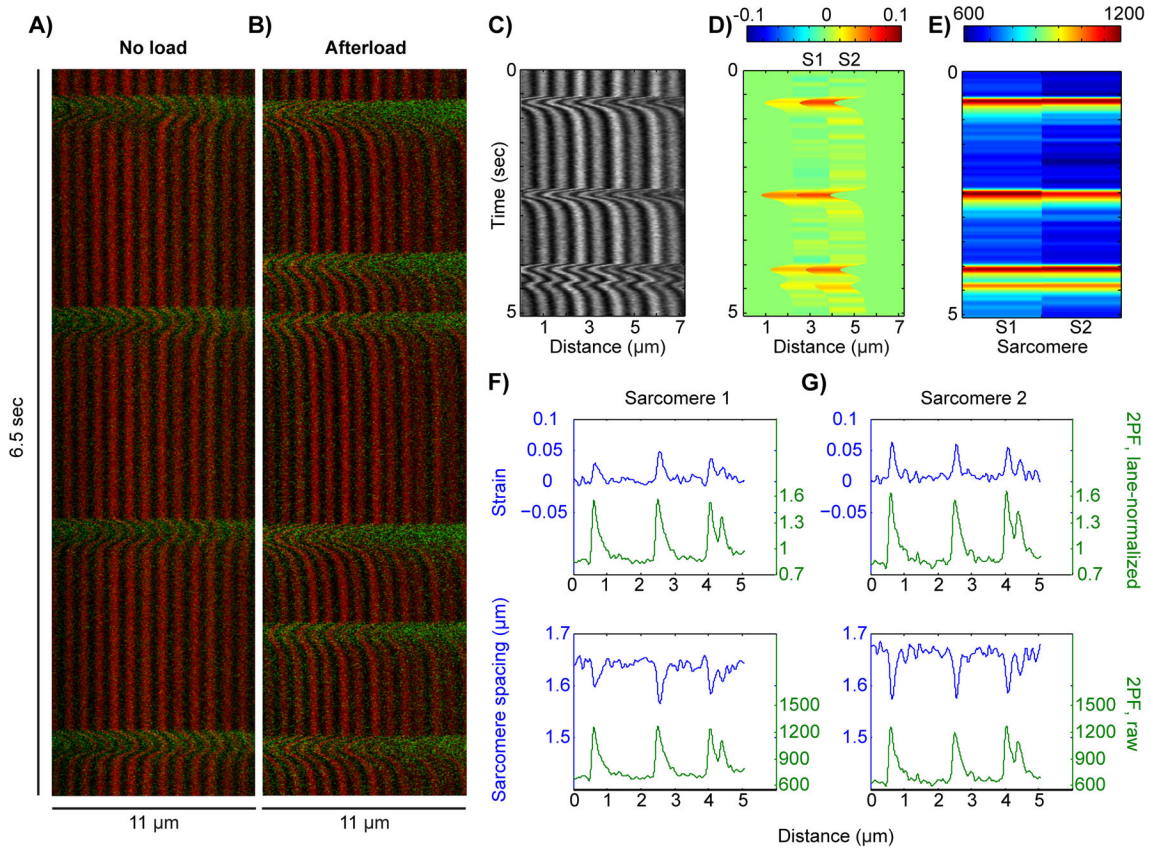

Figure 7.

Multimodal SHG-2PF imaging of cardiac myocytes from transverse aortic constriction (TAC) mice. (A) SHG (red) and 2PF (green) data from an isolated TAC cardiac myocyte under no load, paced at 0.5 Hz. (B) SHG and 2PF data from a TAC cardiac myocyte embedded in a gel to produce afterload, showing calcium tides while being paced at 0.5 Hz. (C–D) Strain map analysis of a localized 2-sarcomere region from a TAC cardiac myocyte under afterload and 0.5 Hz pacing. (E) 2PF signal within the corresponding sarcomeres from (D). (F–G) Plots of sarcomere strain vs. lane-normalized 2PF (top) and sarcomere spacing vs. raw 2PF (bottom).